1. INTRODUCTION

In recent years, the construction materials industry has taken a great interest in the development of innovative cements, which can have important benefits from the point of view of lower energy requirements in production, and lower emission of greenhouse gases (primarily CO_2) compared to the manufacture of Portland cement (Juenger et al., 2011; Pacheco-Torgal, 2015; Provis et al., 2015; Shi et al., 2006). Alkali-activated cements are one of these classes of cement that has attracted significant attention. Alkali-activation requires two basic components: natural or artificial aluminosilicates as the powder precursor, and an alkaline activator. Alkali activated slag (AAS) cements are obtained by mixing ground granulated blast furnace slag, which is an iron industry by-product, with alkaline solutions (Fernández-Jiménez and Puertas, 2003; Shi and Day, 1996).

A large number of parameters can influence the synthesis processes of these AAS cements, such as the type and fineness of the slag, the activating solution/binder ratio, temperature, time, relative humidity, and nature and concentration of the alkali activator (Bernal et al., 2014). The curing duration and environment are critical in determining the microstructure and composition of the reaction products, which will affect the physico-mechanical behaviour of the hardened material. Talling (Talling, 1989) studied the effect of different curing conditions on the performance of AAS pastes, mortars, and concrete. He observed that the AAS mortars and concretes performed very well even after an extremely strong heat treatment followed by storage at a low relative humidity. In addition, at normal temperature, the drop from 100 to 70 % relative humidity did not affect the strength properties of the concrete.

Although these alkali-activated materials can also present performance advantages in some applications compared to Portland cement (PC) (Provis and van Deventer, 2014; Van Deventer et al., 2010), there is not yet sufficient information available about the durability of alkali activated slags, and in particular the interactions between the binder and embedded reinforcing steel rebars. The deterioration of reinforced concrete structures is critical in defining their service behaviour, design life and safety. The main reason for their premature failure is corrosion of the reinforcement. Passivity of reinforcing steel is enabled by the formation of a thin protective surface passive film, which is maintained in high-quality concrete, unless the film is damaged by chloride or by a pH drop of the concrete pore electrolyte, e.g. due to carbonation (Angst et al., 2017; Böhni, 2005).

Blast furnace slags contain sulfur among the minor elements of its composition, which must be viewed carefully because it can influence corrosion process of steel in alkali-activated slag cements, as it is redox-sensitive. In a previous research study (Criado, M. et al., 2018), the stability of steel in a modified alkali-activated blast furnace slag mortar system under exposure to alkaline and alkaline-chloride rich solutions was studied through electrochemical measurements. The mortars presented highly negative corrosion potential and high current density values in the presence of chloride; however, the steel extracted from mortars after 9 months of exposure to high chloride concentrations did not show evident pits or corrosion product layers, indicating that the presence of sulfide supplied by the slag reduces the redox potential in a way which offers protection to the steel.

This work is devoted to study the effect of the curing time (28, 90 and 180 days) on binder development and corrosion resistance of reinforcing steel embedded in alkali-activated slag cements activated by sodium silicate.

2. EXPERIMENTAL METHODOLOGY

The raw material used in this study was a blast furnace slag supplied by Ecocem (France), with a Blaine fineness of 506 ± 22 m^2/kg and an average particle size of 11.2 ± 0.1 µm. The activating solution used to make pastes and mortars was 7 wt.% sodium metasilicate, i.e. 7 g of Na_2SiO_3 per 100 g of slag, at a water to total solids (slag + Na_2SiO_3) mass ratio of 0.40. The solution was prepared from laboratory reagent grade sodium metasilicate powder (Na_2SiO_3) supplied by Sigma-Aldrich. A CEN standard sand (BS EN 196-1:2005, 2005) was used to prepare mortars, at a sand/binder mass ratio of 3.0. The pastes and mortars were sealed with cling film and stored at 20±2°C for 28, 90 and 180 days.

Mortars were cast as cube (50 x 50 x 50 mm) and disc (100 mm diameter and 50 mm height) specimens, for mechanical and chloride migration testing respectively. 14 prismatic mortar specimens (80 x 50 x 50 mm), each with two embedded steel rebars (12 mm diameter and 100 mm length) and a very low cover depth to minimise transport effects and enable very rapid contact between the steel and the exposure

solution, were also prepared for the electrochemical tests. The rebars were mild corrugated steel according to British standard usage (BS 4449:2005+A3:2016, 2005), whose chemical composition (% by weight) was 0.18-0.22 C, 0.23 Si, 0.76 Mn, 0.04 P, 0.03 S, 0.13 Cr, 0.20 Ni, 0.47 Cu, 0.02 Mo, and balance Fe. The as-received reinforcement was sectioned into rods with the rust layer intact, and these were embedded in mortars, with the ends masked with epoxy resin (Sikagard-62) coating to leave an exposed surface area of 10 cm^2. Reinforced prismatic mortars, upon reaching the specified time of curing (28, 90 or 180 days), were exposed to an alkaline and chloride-rich solution, 1 M NaOH + 3.5 wt.% NaCl (denoted Cl), and to standard laboratory conditions with open storage (denoted SL) until the specimen reached one year from its manufacture. Measurements of pH were performed throughout the test, and a pH value of about 13.5-14 was maintained throughout.

X-ray diffraction (XRD) was carried out in a Bruker D2 Phaser instrument with Cu-Kα radiation and a nickel filter. The tests were conducted with a step size of 0.02° and a counting time of 1.1 s/step, from 5° to 60° 2θ.

The compressive strengths of mortars were determined by testing triplicate cubic samples with a loading speed of 0.25 MPa/s, in an automatic testing machine (Controls Automax5).

Non-steady state chloride migration was determined via the Nordtest NT Build 492 method (NTBuild 492, 1999). In the procedure, duplicate disk samples were used.

The corrosion resistance of AAS mortars was evaluated by electrochemical tests such as corrosion potential (E_{corr}) and polarisation curves, up to 360 days after mixing of the mortar. A conventional three-electrode cell was used, where the steel rebars embedded in the slag mortars acted as working electrodes, and a stainless steel cylinder of 5 cm of diameter (acting as counter electrode) was placed above the mortars. The counter electrode had a centrally drilled hole in which an Ag/AgCl (filled with 3 M KCl) electrode was placed to act as the reference electrode. A pad soaked in tap water was interposed between these electrodes and the mortar surface to facilitate the electrochemical measurements. The electrochemical characterisation for the mortars was performed using a Princeton Applied Research VersaSTAT 3F. At 360 days after mixing the mortars, anodic polarisation curves were recorded, at a scan rate of 0.1667 mV s^{-1}.

3. RESULTS AND DISCUSSION

3.1 Mineralogical characterisation of alkali-activated slag pastes

X-ray powder diffraction patterns for the anhydrous slag and the AAS pastes cured for 28, 90 and 180 days are shown in Figure 1. The diffractograms of the anhydrous slags show mainly an amorphous phase, indicated by a wide and diffuse reflection in the range 23º-36º 2θ. The diffractograms of the alkali-activated slag pastes confirmed the formation of calcium silicate hydrate (C-S-H) type gel (PDF # 33-0306, and almost certainly with some substitution of Na and Al into the C-S-H structure) as the main reaction product in all samples. Over the time of curing, sharpening and intensification of the peaks assigned to the C–S–H type gel (29.5° and 49.8°) can be identified as the system achieved a higher degree of reaction. However, the peak at 29.5° became more intense at 28 days, because calcite was also detected in the samples, and its main diffraction peak overlaps with that of the C-S-H type gel at this angle. The amount of calcite formed decreased with time, and therefore the main peak intensity was less at 90 days than at 28 days.

The main secondary products formed in these pastes were layered double hydroxide with a hydrotalcite type structure ($(Mg_{0.667}Al_{0.33})(OH)_2(CO_3)_{0.137}(H_2O)_{0.5}$) (PDF # 89-0460). Several peaks can be seen at 32.5º, 37.9º, 45.9º and 51.9º which are assigned to a hydrogarnet phase resembling hibschite ($Ca_3Al_2Si_2O_8(OH)_4$) (PDF # 73-1654, a member of the katoite-like solid solution series with silicate/hydroxyl substitution). The amount of hydrotalcite formed increased over the curing time, while the percentage of hibschite hydrogarnet decreased. The formation of hydrotalcite is favoured, which reduces the aluminium available in the system, and consequently can hinder the formation of hydrogarnet type phases (Bernal et al., 2014).

Calcium carbonates such as calcite (PDF # 86-2334), vaterite (PDF # 72-0506) and aragonite (PDF # 03-1067) (all polymorphs of $CaCO_3$) are also observed in all pastes. The reflections assigned to vaterite and aragonite remained almost unchanged with the time, but those assigned to the calcite decreased.

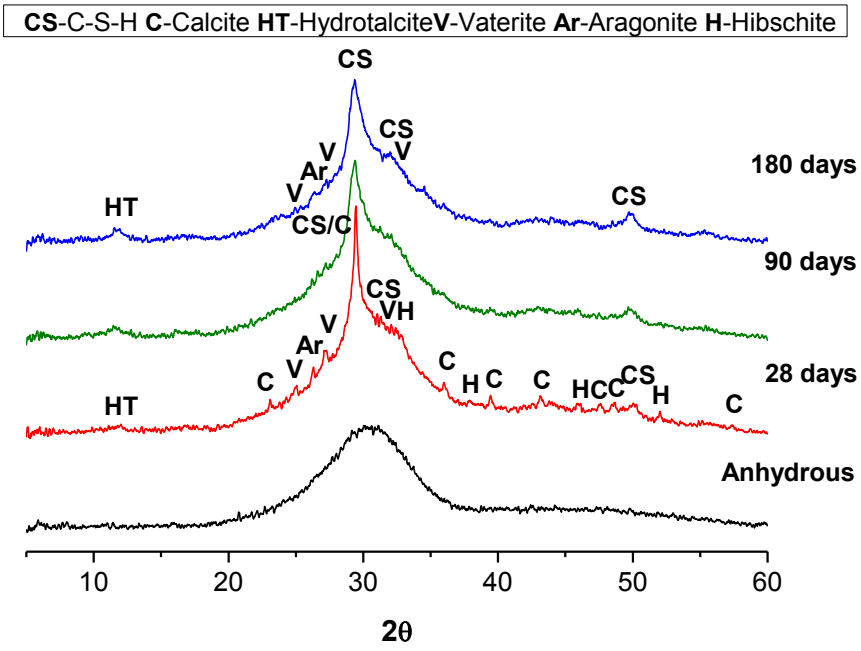

Figure 1. XRD patterns of the anhydrous and alkali-activated slags over time.

3.2 Physical and mechanical properties of alkali-activated slag mortars

The compressive strengths of AAS mortars after 28, 90 and 180 days of curing are depicted in Figure 2. The compressive strength increased over time; the formation of denser C-S-H type gels was favoured with advancing curing time, and a higher mechanical strength development was reached at 180 days, although the 28-day strength of almost 80 MPa is nonetheless notable.

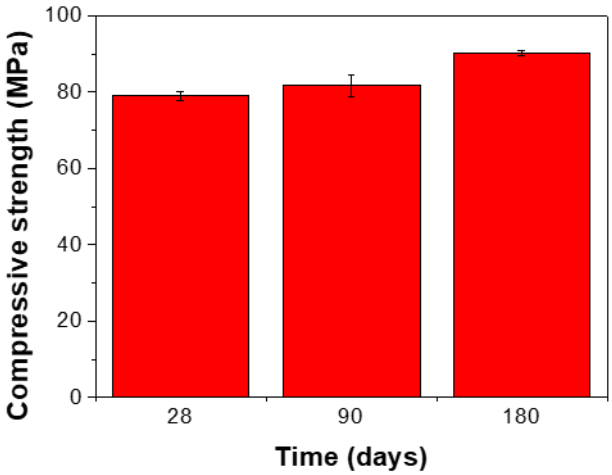

Figure 2. Compressive strength evolution over time for mortar cubes

Figure 3 shows the chloride migration coefficient determined for AAS mortars after 28, 90 and 180 days of curing. This coefficient decreased with the curing time due to the densification of C-S-H type gels within the microstructure, causing a deceleration of chloride migration through the pore network of the specimens.

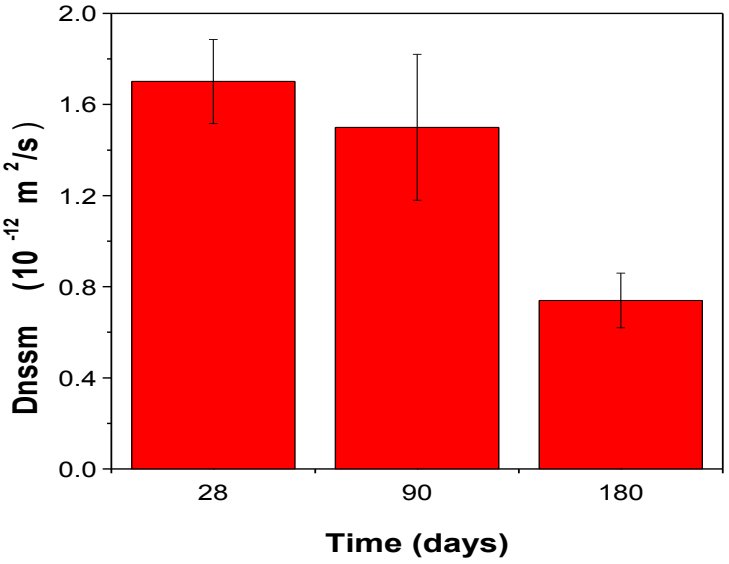

Figure 3. Change in chloride migration coefficient D_{nssm} over time

3.3 Electrochemical measurements

Figure 4 shows corrosion potential (E_{corr}) values of steel embedded in slags mortars exposed to standard laboratory conditions (SL) and to alkaline chloride-rich solution (Cl) as a function of time after mixing: 28, 90 and 180 days. The steel embedded in the mortars exposed to standard laboratory conditions showed E_{corr} values between – 0.104 and 0.047 V vs. Ag/AgCl, indicating that the steel was in a passive state (ASTM C876-15, 2015). In the alkaline chloride-rich solution, E_{corr} values decreased with time, and in the same way independent of the time after mixing for each different exposure age (marked with dashed vertical lines in Figure 4). Finally, all samples independent of the curing time presented E_{corr} values of around -0.450 V vs. Ag/AgCl at 360 days after mixing of the mortars. Such negative values of potential are commonly taken to indicate a high probability of corrosion, attributed to the breakdown of the passive film induced by the chloride ions. However, this interpretation does not account for the effects of sulfide, which is also a strong reductant but does not necessarily cause corrosion of steel in AAS mortars (Criado et al., 2018).

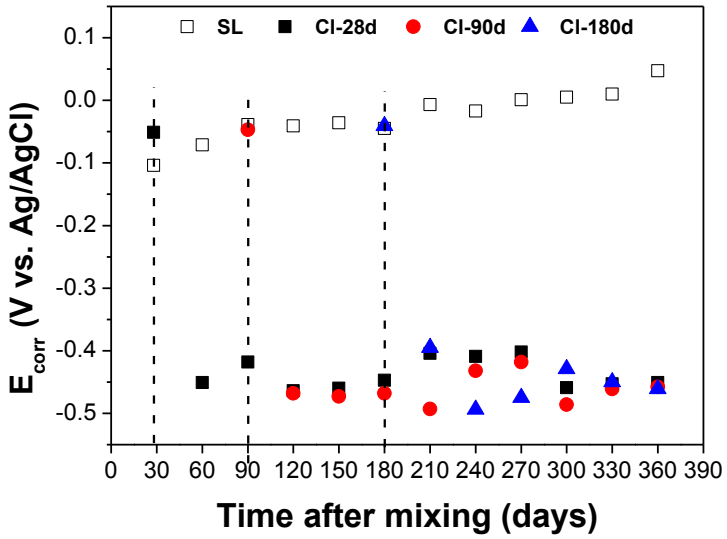

Figure 4. Evolution of the corrosion potential over time exposed to standard laboratory conditions (SL) and alkaline chloride-rich solutions (Cl), where exposure started after 28, 90 and 180 days of mortar mixing (marked with vertical dashed lines).

Figure 5 shows anodic polarisation curves recorded for the steel embedded in AAS specimens exposed to standard laboratory conditions (SL) and alkaline and chloride-rich solution (Cl) up to 360 days after mixing of the mortars. The steel embedded in slag mortars exposed to standard laboratory conditions presented E_{corr} values around +0.042 V vs. Ag/AgCl and corrosion current density (i_{corr}) values around 0.07 µA cm^{-2}, indicating that the steel was in a passive state (Andrade et al., 1986). In the alkaline chloride-rich solution, the anodic curves showed higher i_{corr} values, in the range from 0.4 to 0.8 µA cm^{-2}, and more negative E_{corr} values, around -0.462 and -0.479 V vs. Ag/AgCl. If such electrochemical parameters were observed in Portland cement-based binders, this would be taken to indicate that the surface passive film on the steel suffered degradation due to the presence of chlorides and the steel presented a high level of corrosion (Andrade et al., 1986). However, in these samples an active/passive transition with a passive potentials in the range -0.360 V and -0.100 V vs. Ag/AgCl was observed, likely associated with the transformation of S^{2-} (Criado, M et al., 2018). The following section will address this point, and the accompanying implicit assumptions, in more detail.

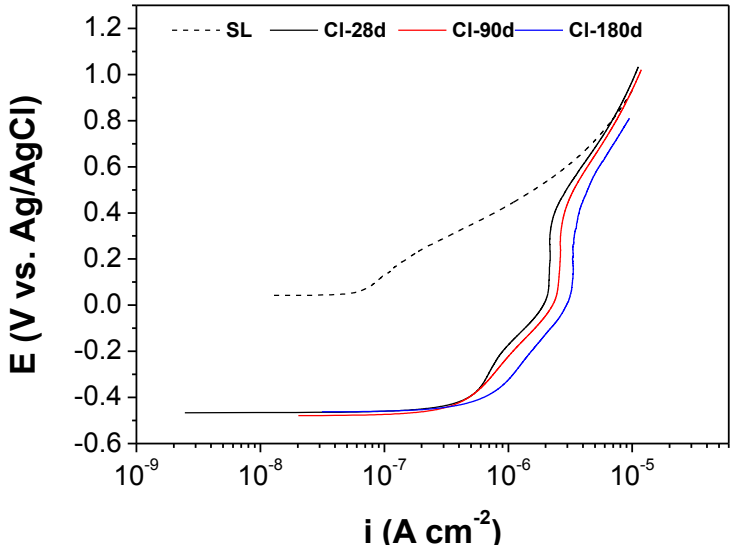

Figure 5. Anodic polarisation curves recorded for slag mortars at 360 days after mortar mixing and exposed to standard laboratory conditions (SL) and alkaline chloride-rich solutions (Cl)

3.4 Surface analysis

Figure 6 shows photographs of the steel rebar specimens extracted from slag mortars that had been immersed in the alkaline chloride-rich solution, to directly visualise the corrosion attack after 360 days of mortar mixing next to the original rebar. The original rebar showed a rust layer, with small regions of reddish stains distributed randomly in its surface. All steel specimens extracted from the specimens presented these same stains, but did not show any evidence of pits or corrosion product layers. The surface aspect of the steels was similar regardless of the curing time of the mortar prior to the start of chloride exposure.

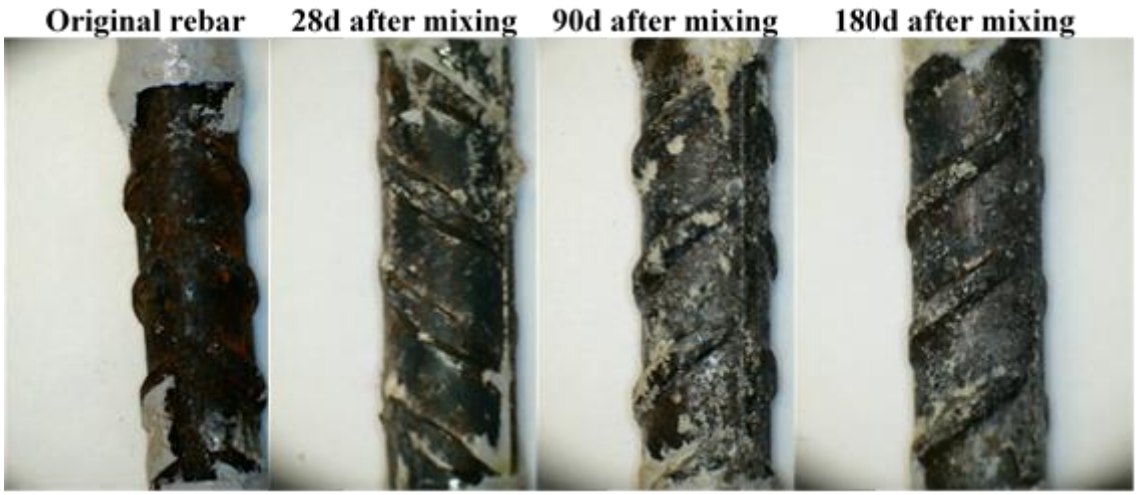

Figure 6. Surface aspect of the original steel rebar and the steel rebars extracted from alkali-activated slag mortars at the end of anodic polarisation curve determination, 360 days after mortar mixing, where the chloride exposure started in each case at the time specified on the respective photograph.

This shows that the corrosion state determination (or estimation) based on the conventional electrochemical measurements, and the corrosion activity observed in the rebar do not have a direct relationship. These discrepancies are attributed to the presence of sulfide in the chemical composition of the slags; as has been discussed previously, the presence of sulfide can significantly reduce the redox potential of the pore solution around the rebar (Criado, M. et al., 2018; Criado and Provis, 2018), and subsequently can alter the nature of the passive film formed on a steel surface, forming a complex iron sulfide layer (Criado, M et al., 2018).

On the other hand, the high corrosion current densities obtained in polarisation curves for the steel elements embedded in the mortar and immersed in alkaline chloride-rich solution indicate that a rather high current is flowing. However, this is not due to corrosion process taking place, but rather the oxidation of HS^- species in the pore solution (Mundra et al., 2017), and therefore, misrepresentative conclusions about the corrosion resistance of reinforcing steel in alkali activated slag mortars would have been obtained if relying solely on conventional electrochemical methods, as these are not able to distinguish rebar oxidation (corrosion) from sulfide oxidation within the cement pore solution (that does not involve a corrosion process).

4. CONCLUSIONS

The main reaction products formed in alkali-activated blast furnace slag mortars were C-A-S-H gel and hydrotalcite. The formation of both products was favoured with the increase of curing time, leading a densification of the matrix.

An increase of curing time led to an increase in compressive strength and a decrease in diffusion coefficients.

Regarding the corrosion resistance of embedded steel rebar, the presence of sulfide anions can significantly reduce the redox potential of the pore solution around the rebar, where a complex iron sulfide layer could be formed. This appears to hinder the corrosion process, meaning that low potentials and high currents observed in conventional electrochemical testing do not necessarily represent actual steel corrosion processes in reinforced alkali-activated slag mortars.

5. ACKNOWLEDGEMENTS

The research leading to these results received funding from the European Research Council under the European Union's Seventh Framework Programme (FP/2007-2013) / ERC Grant Agreement #335928. The authors would like to acknowledge the technical support provided by Dr Oday Hussein, and thank

Mr Kieran Nash at The University of Sheffield for supplying the rebars. This research was performed in part at the MIDAS Facility, at The University of Sheffield, which was established with support from the Department of Energy and Climate Change.

6. REFERENCES

Andrade, C., Castelo, V., Alonso, C., Gonzalez, J.A., 1986. The determination of the corrosion rate of steel embedded in concrete by the polarization resistance and AC impedance methods, STP18302S Corrosion effect of stray currents and the techniques for evaluating corrosion of rebars in concrete. ASTM International, West Conshohocken, PA, pp. 43-63.

Angst, U.M., Geiker, M.R., Michel, A., Gehlen, C., Wong, H., Isgor, O.B., Elsener, B., Hansson, C.M., François, R., Hornbostel, K., Polder, R., Alonso, M.C., Sanchez, M., Correia, M.J., Criado, M., Sagüés, A., Buenfeld, N., 2017. The steel–concrete interface. Mater Struct 50(2), 143.http://dx.doi.org/10.1617/s11527-017-1010-1

ASTM C876-15, 2015. Standard test method for corrosion potentials of uncoated reinforcing steel in concrete, ASTM international, West Conshohocken, PA.

Bernal, S.A., San Nicolas, R., Myers, R.J., Mejía de Gutiérrez, R., Puertas, F., van Deventer, J.S.J., Provis, J.L., 2014. MgO content of slag controls phase evolution and structural changes induced by accelerated carbonation in alkali-activated binders. Cem. Concr. Res. 57, 33-43.http://dx.doi.org/10.1016/j.cemconres.2013.12.003

Böhni, H., 2005. Corrosion in reinforced concrete structures. Woodhead Publishing Ltd., Abington Cambridge, England.

BS 4449:2005+A3:2016, 2005. Steel for the reinforcement of concrete. Weldable reinforcing steel. Bar, coil and decoiled product. Specification, Comittee Reference ISM/104.

BS EN 196-1:2005, 2005. Methods of testing cement. Part 1: Determination of strength, British Standards Institute: London. pp. 1-36.

Criado, M., Bernal, S.A., Garcia-Triñanes, P., Provis, J.L., 2018. Influence of slag composition on the stability of steel in alkali-activated cementitious materials. J Mater Sci 53, 5016-5035.http://dx.doi.org/10.1007/s10853-017-1919-3

Criado, M., Mundra, S., Bernal, S., Provis, J., 2018. Influence of Sulfide on the Onset of Chloride-Induced Corrosion of Steel Reinforcement in Alkali-Activated Slags, Durability of Concrete Structures. Whittles Publishing, pp. 149-153.

Criado, M., Provis, J.L., 2018. Alkali Activated Slag Mortars Provide High Resistance to Chloride-Induced Corrosion of Steel. Frontiers in Materials 5(34), 1-15.http://dx.doi.org/10.3389/fmats.2018.00034

Fernández-Jiménez, A., Puertas, F., 2003. Effect of activator mix on the hydration and strength behaviour of alkali-activated slag cements. Adv. Cem. Res. 15(3), 129-136.http://dx.doi.org/10.1680/adcr.2003.15.3.129

Juenger, M., Winnefeld, F., Provis, J.L., Ideker, J.J.C., research, c., 2011. Advances in alternative cementitious binders. 41(12), 1232-1243

Mundra, S., Bernal, S.A., Criado, M., Hlaváček, P., Ebell, G., Reinemann, S., Gluth, G.J., Provis, J., 2017. Steel corrosion in reinforced alkali-activated materials. RILEM Technical Letters 2, 33-39

NTBuild 492, 1999. Concrete, mortar and cement-based repair materials: chloride migration coefficient from non-steady-state migration experiments. Nortest method, Espoo, Finland.

Pacheco-Torgal, F., 2015. Introduction to handbook of alkali-activated cements, mortars and concretes, Handbook of alkali-activated cements, mortars and concretes. Elsevier.

Provis, J.L., Palomo, A., Shi, C., 2015. Advances in understanding alkali-activated materials. Cem. Concr. Res. 78, Part A, 110-125.http://dx.doi.org/10.1016/j.cemconres.2015.04.013

Provis, J.L., van Deventer, J.S., 2014. Alkali Activated Materials, State of the Art Report of RILEM TC 224-AAM. Springer, Dordrecht, the Netherlands.

Shi, C., Day, R.L., 1996. Some factors affecting early hydration of alkali-slag cements. Cem. Concr. Res. 26(3), 439-447.http://dx.doi.org/10.1016/S0008-8846(96)85031-9

Shi, C., Roy, D., Krivenko, P., 2006. Alkali-activated cements and concretes. CRC press.

Talling, B., 1989. Effect of curing conditions on alkali-activated slags. ACI Collection 114, 1485-1500

Van Deventer, J.S.J., Provis, J.L., Duxson, P., Brice, D.G., 2010. Chemical Research and Climate Change as Drivers in the Commercial Adoption of Alkali Activated Materials. Waste Biomass Valori. 1(1), 145-155.http://dx.doi.org/10.1007/s12649-010-9015-9